

Complexation Dynamics of Calcium Ion in Chitosan Monomer: A Theoretical Assessment from the Gas-Phase to Microsolvation Environments

Lilian Tatiane F. M. Camargo,^{a,b} Wilson Roberto Lopes Filho,^a Flávio O. Shances Neto,^c
Nayara D. Coutinho^{id}^d and Ademir João Camargo^{id}*,^a

^aGrupo de Química Teórica e Estrutural de Anápolis, Centro de Pesquisa e Pós-Graduação,
Universidade Estadual de Goiás, 75132-400 Anápolis-GO, Brazil

^bInstituto Federal de Educação, Ciência e Tecnologia de Goiás, 75131-457 Anápolis-GO, Brazil

^cInstituto Federal de Educação, Ciência e Tecnologia de Goiás, 72876-601 Valparaíso de Goiás-GO, Brazil

^dFaculdade SENAI Roberto Mange, Serviço Nacional de Aprendizagem Industrial-SENAI,
75113-630 Anápolis-GO, Brazil

This study investigates the interaction between calcium ions and glucosamine molecules (GlcN) gas-phase and the interaction of calcium ion with GlcN in the microsolvation environments using Car Parrinello molecular dynamics and density functional theory. Our findings reveal stable complexation between GlcN and calcium ions at various molecular sites in gas-phase and in the microsolvation environments. Furthermore, the Quantum Theory of Atoms in Molecules (QTAIM) analyses indicate a predominantly ionic character for all interactions in both gas-phase and microsolvation systems. The Natural Bond Orbital analyses demonstrate that the calcium ion serves as an electron acceptor, receiving lone pairs of electrons from oxygen and nitrogen atoms for its vacant orbitals. A comprehensive understanding of GlcN-calcium-water interactions at the molecular level can contribute to new research directions and applications for chitosan and its monomer, glucosamine, in the pharmacological domain.

Keywords: glucosamine, Car-Parrinello molecular dynamics, DFT, ion calcium

Introduction

Calcium permeable ion channels are a regulator of a diverse set of cellular events, such as muscle contraction, neurotransmitter release, transport molecules, cellular proliferation, and cell death.^{1,2} Medicinal studies have associated the dysregulated calcium metabolism with autism spectrum disorders,³ developing prostate,^{4,5} and breast cancers,² neurodegenerative pathologies,⁶ and as a cause of cardiovascular diseases such as myocardial infarction.^{7,8}

The search for natural components that may prevent and treat diseases has highlighted chitosan, a nontoxic biopolymer that is a partially deacetylated derivative of chitin.⁹ Chitosan has hydroxyl and amine-reactive functional groups in its structure, which may ensure its bioactivities, such as its antimicrobial and anti-inflammatory activity, hypocholesterolemia effect, and drug delivery.¹⁰⁻¹⁴ Its excellent ability to bind cations¹⁵ has

been explored to deliver and release bioactive molecules in the gastrointestinal tract: chitosan chelate Ca²⁺ improves the adsorption of these ions by the intestine.¹⁶ In addition to medical and food applications, chitosan has attracted considerable interest in agriculture¹⁷ and environmental industries, due to the manufacture of materials with a low impact on nature, in the form of films, hydrogel and fibers¹⁸⁻²⁰ and in the removal of heavy metals from water.²¹⁻²³

Chitosan is a linear polysaccharide composed of β -1,4-linked D-glucosamine (GlcN) and *N*-acetyl-D-glucosamine.¹⁷ Here, we choose to study chitosan monomer, the GlcN (Figure 1), which has many pharmacological applications^{24,25} including anti-inflammatory and immunomodulatory therapy, neuroprotective effect, treatment of osteoarthritis,^{25,26} cardiovascular diseases^{7,24} neurodegenerative pathology,⁶ bacterial infection,²⁷ and anti-tumoral activities.²⁴

From a theoretical point of view, several computational approaches have provided insights into the interaction of chitosan, GlcN, and their derivatives with metallic cations.²⁸⁻³⁴ Fattahi *et al.*²⁹ used the B3LYP/6-311++G**

*e-mail: ajc@ueg.com.br

Editor handled this article: Paula Homem-de-Mello (Associate)



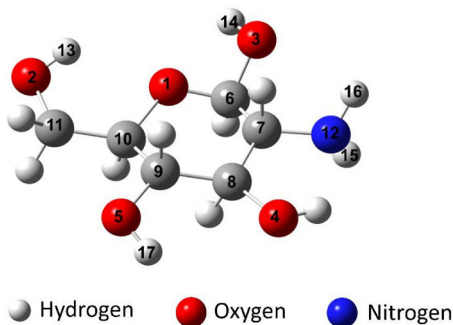


Figure 1. GlcN molecular structure and atomic numbering used in the calculations.

calculation level of theory to study the complexation of GlcN with monovalent (Li^+ , Na^+ , K^+) and bivalent (Mg^{2+} , Ca^{2+} and Zn^{2+}) cations. The results showed that monovalent ions form bidentate coordination and bivalent ions tetradentate coordination.

Gomes *et al.*³⁰ also studied the interaction of GlcN with monovalent and divalent metals, namely Ni^+ , Ni^{2+} , Cu^+ , Cu^{2+} , Zn^+ , and Zn^{2+} cations, using the B3LYP/6-31G** level of theory in the absence and the presence of water. The calculations have shown that in the gaseous phase, the most stable complex with monovalent cations is that with Ni^+ in the form of bidentate interaction with an amino group and hydroxyl oxygen. In the case of the divalent cations, Zn^{2+} and Ni^{2+} produce tridentate complexes with GlcN, binding with two hydroxyl oxygen and the ring oxygen. On the other hand, the complexation of GlcN and Cu^{2+} was stable in two configurations, the first one binding with two hydroxyl oxygen and the ring oxygen and the second one interacting with the amino group and hydroxyl oxygen. For the hydrated metal-GlcN, the configuration where ions were bound to the amino and a neighboring hydroxyl group provided more favorable complexes.

Hassan *et al.*³¹ using B3LYP/6-31G level of theory, studied the complexation of Pb^{2+} ions with chitosan monomer. The results showed the coordination of Pb^{2+} ions on different sites depending upon the initial position. The most stable complexation was binding Pb^{2+} with two GlcN's hydroxyl oxygen. In another study, Hassan *et al.*,³² using B3LYP/LanL2DZ, observed the complexation preference of Hg^{2+} with nitrogen and neighboring hydroxyl group of the GlcN. The results have shown that the presence of water molecules slightly affects the most favorable binding configuration and strongly stabilizes the metallic complexes by forming several hydrogen bonds.

The strategy that we followed to assess the complexation of the GlcN with the calcium cation in the gas-phase and aqueous microsolvation environment was to use the Car-Parrinello molecular dynamics (CPMD). To understand the nature of the chemical bond and stabilization energy of the

complexes, we performed the Quantum Theory of Atoms in Molecules (QTAIM) and Natural Bond Orbital (NBO) analyses from snapshot structures taken from the *ab initio* molecular simulations.

Methodology

Molecular dynamics

The anomeric α and β forms of GlcN are possible. The α form is predominantly protonated at the amino group (GlcN^+), while the β form is primarily non-protonated (GlcN).³⁵ In this study, the analyses were conducted with the neutral β -GlcN, which is significantly present in biological systems.³⁴

All the Car-Parrinello molecular dynamics (CPMD) simulations were carried out using the CPMD 4.1 package.³⁶ The electronic structure was treated within the generalized gradient approximation to density functional theory (DFT),³⁷ using the Perdew-Burke-Ernzerhof (PBE) exchange-correlation functional.³⁸ The core was described using the norm-conserving Troullier and Martins pseudopotentials.³⁹ The Kohn-Sham orbitals were expanded with a plane wave cutoff of 75 Ry and cutoff energy of 300 Ry for the charge density expansion. The fictitious electronic mass was set to be 400 a.u. with a time step of 4.0 a.u. The wavefunction optimizations for all systems were carried out using the direct inversion in the iterative subspace algorithm (ODIIS).⁴⁰ For the Brillouin zone sampling, only gamma points were used. The ionic temperature and the electronic fictitious kinetic energy were controlled by a chain of three Nose-Hoover thermostats^{41,42} at 300 K. Simulations were performed in both the gas and the microsolvated environments. For the gas phase, one GlcN molecule and one calcium ion were placed inside a 16 Å cubic cell, and periodic boundary conditions were imposed for each trajectory. Four different initial configurations were built in order to account the possible interactions between Ca^{2+} and the main active sites of GlcN ($-\text{OH}$ and $-\text{NH}_2$ groups) as proposed by Jeremić *et al.*³³ The initial configurations ((GlcN- Ca^{2+} (1), GlcN- Ca^{2+} (2), GlcN- Ca^{2+} (3), and GlcN- Ca^{2+} (4)) can be seen in Figure 2. Under these conditions, a total simulation time of 29 ps was performed for each trajectory. To account for the aqueous micro-solvation effect in the complexation of calcium by GlcN, two simulations were performed. The initial configurations GlcN- Ca^{2+} (2), and GlcN- Ca^{2+} (3) were selected, and in each one, 12 water molecules were added. These simulations were run using the same molecular dynamics parameters as used in a gas-phase environment. All CPMD inputs were created with the Transitivity Code-

version 1.0.1.⁴³ Details of the computational program can be found on the literature.⁴⁴

Stationary electronic structure calculations

All the DFT calculations were carried out with the Gaussian 09 package.⁴⁵ To obtain the complexation energy, we selected 100 equally spaced uncorrelated snapshots for each one of the molecular dynamics simulations after the equilibration of the complexation. In this study, we calculated the electronic structure for each of the 100 structures using the M06-2X/6-311++G(d,p) level of theory.⁴⁶ To account for dispersion effects, we corrected the energies using the Petersson-Frisch empirical dispersion term.⁴⁷

The interaction energies for complexation between GlcN and the calcium ion were corrected for the basis set superposition error (BSSE) based on the counterpoise correction method,^{47,48} using equation 1:

$$E_{\text{int}} = E_{\text{GlcN-Ca}^{2+}} - (E_{\text{GlcN}} + E_{\text{Ca}^{2+}}) \quad (1)$$

where E_{int} represents the electronic energy of interaction between calcium ions and GlcN, $E_{\text{GlcN-Ca}^{2+}}$ is the electronic energy of complex, E_{GlcN} and $E_{\text{Ca}^{2+}}$ are the electronic energies of GlcN and calcium ion gas-phase, respectively. The deformation of the complexation was considered for each fragment. In the cases of the ion calcium-GlcN-water complexes, the interaction energies were calculated as:

$$E_{\text{int}} = E_{\text{GlcN-Ca}^{2+}-(\text{H}_2\text{O})_n} - (E_{\text{GlcN}} + E_{\text{Ca}^{2+}} + nE_{\text{H}_2\text{O}}) \quad (2)$$

where $E_{\text{GlcN-Ca}^{2+}-(\text{H}_2\text{O})_n}$ stands for energy for the complex between calcium ion, GlcN, and n water molecules that complex, and E_{GlcN} , $E_{\text{Ca}^{2+}}$ and $E_{\text{H}_2\text{O}}$ are the total energy for separate fragments. Each of the complexes' interaction energy was obtained by the average complexation energies of all uncorrelated snapshots.

To understand the nature of interactions and charge distribution, a set of Quantum Theory of Atoms in Molecules (QTAIM)⁴⁹ and Natural Bond Orbital (NBO)⁵⁰ calculations were performed. For QTAIM analysis, two snapshots were chosen between the equilibrium of complexation and the final time of simulation: one with the shortest and the other with the most extended interaction distances, which were carried out using the Multiwfn3.3.7⁵¹ software. For NBO analysis, one snapshot was chosen corresponding to the lowest complexation energy. The hyperconjugation interaction energy between an occupied (i) and an unoccupied (j) orbitals was calculated according to Second-Order Perturbation Theory, as described in

equation 3:

$$E^{(2)} = -h_i \frac{\langle \phi_i | F | \phi_{j^*} \rangle^2}{\epsilon_{j^*} - \epsilon_i} = -n_i \frac{F_{(ij)}^2}{\Delta E} \quad (3)$$

where n_i is the population occupation of the σ donor orbital, $\langle \phi_i | F | \phi_{j^*} \rangle$ and $F_{(ij)}^2$ are the NBO Fock matrix element between i and j natural bond orbital, $\epsilon_{j^*} - \epsilon_i$ is the difference between the energy of the antibonding orbital j^* and the energy of the bonding orbitals i .

Results and Discussion

Molecular dynamics simulations

Gas-phase

Four initial configurations between GlcN and Ca^{2+} (GlcN-Ca^{2+} (1), GlcN-Ca^{2+} (2), GlcN-Ca^{2+} (3), and GlcN-Ca^{2+} (4)) that could lead to the formation of a stable complex were simulated by the Car-Parrinello molecular dynamics approach. The snapshots of trajectories for all the initial configurations at 300 K are illustrated in Figure 2. At 0 ps, the labeling scheme and geometric parameters for initial molecular configurations of Ca^{2+} and GlcN are presented (GlcN-Ca^{2+} (1), GlcN-Ca^{2+} (2), GlcN-Ca^{2+} (3), and GlcN-Ca^{2+} (4)). A clearer view of the formation of the interactions between GlcN and Ca^{2+} are shown in Figure 3, with evolution in time of the bond lengths formed between calcium and different main sites of GlcN. The complexation energies for all complexes studied were calculated by the average of the complexation energies of 100 uncorrelated snapshots. The frames were selected after equilibration of complexation.

In the GlcN-Ca^{2+} (1) configuration, the Ca^{2+} was initially positioned at 2.85 Å from N12 and 4.50 Å from O3 atoms of GlcN. After about 300 fs of the simulation, an interaction was formed by the approximation of Ca^{2+} on the N12 (Figures 2 and 3). After 0.7 ps, the bidentate contact was formed by binding between Ca^{2+} and O3, and almost at 3.7 ps, a third interaction was observed by the O2 atom, which was approaching the Ca^{2+} forming a tridentate stable complex (Ta_N2O) that remained in equilibration until the end of the simulation, in form of pyramidal geometry with average complexation energy of $-681.51 \text{ kJ mol}^{-1}$.

In the GlcN-Ca^{2+} (2) initial configuration, the calcium ion was first positioned close to two -OH groups: at 3.45 Å from O2 and 3.37 Å from O3. Almost 200 fs, bidentate interactions were formed simultaneously by the binding of Ca^{2+} with O2 and O3. After 400 fs, Ca^{2+} interacts with O1, leading to a tridentate pyramidal species which survives for 1.4 ps, when by the binding of O4, a four-coordinate

seesaw geometry (Fc_4O) was formed (Figures 2 and 3). It remained in equilibrium until the end of the simulation, which obtained the average complexation energy of $-794.53 \text{ kJ mol}^{-1}$.

In the third initial configuration, GlcN-Ca²⁺ (3), the calcium ion was initially positioned at 4.92 Å of O2 and 3.68 Å of O5 sites of GlcN. The interaction with O5 occurs quickly, about 200 fs, and shortly after that (300 fs), the hydrogen of the hydroxyl group (H17) was transferred to N12, protonating the amino group. It was only after 18.6 ps that O2 bound with Ca²⁺, resulting in a bidentate complex (Bi_2O) forming a hexagonal ring with GlcN that remained in equilibration until the end of the simulation (Figures 2 and 3). The average complexation energy for this bidentate complex was $-781.60 \text{ kJ mol}^{-1}$.

In GlcN-Ca²⁺ (4), Ca²⁺ was initially positioned at 3.31 Å from O5 and 3.79 Å from N12, as shown in Figure 2. At about 100 fs, the calcium ion bound with O5,

at around 242 fs with N12 and around 532 fs with O1, forming a second stable tridentate complex Tb_N2O of pyramidal geometry (Figures 2 and 3), which remained in equilibration until the end of the simulation with average complexation energy of $-680.50 \text{ kJ mol}^{-1}$.

These simulations showed that the adsorption of a calcium ion by GlcN in the gas-phase environment occurred in different sites of GlcN, leading to the formation of complexes with different geometries, coordination numbers, and stabilities. The most stable complex was Fc_4O, because of its four bonds between GlcN sites and Ca²⁺. The second most stable was the bidentate complex, in which hydrogen was transferred from hydroxyl to the amino group (Bi_2O) followed by the tridentate complex formed by binding between two hydroxyls and one nitro group (Ta_N2O). The least stable was a tridentate complex-forming by binding with the heteroatom, one hydroxyl group, and the amino group (Tb_N2O).

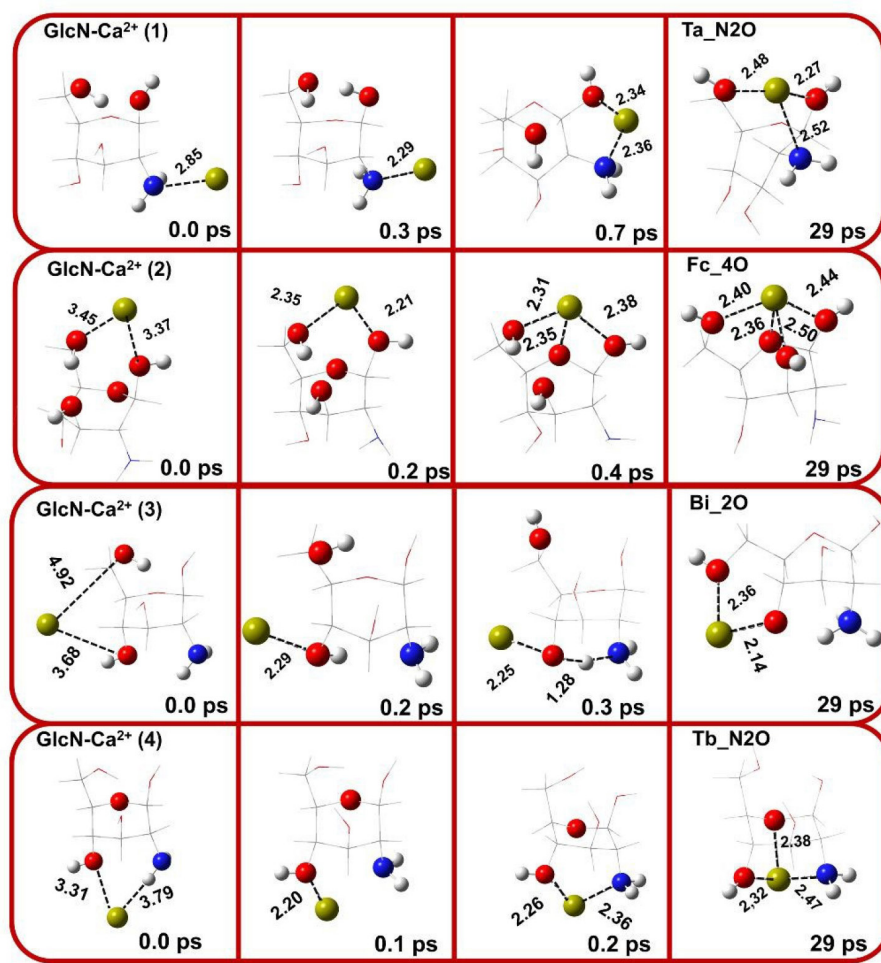


Figure 2. The geometrical parameters are depicted at four different time points during the Car-Parrinello Molecular Dynamics simulation for four distinct initial configurations: GlcN-Ca²⁺ (1), GlcN-Ca²⁺ (2), GlcN-Ca²⁺ (3), and GlcN-Ca²⁺ (4). These parameters illustrate the approach of the calcium ion towards the glucosamine sites throughout the simulation. At 29 ps, the bond distances represent the average interaction distance (in Å) between the initial time of complex formation (complexation equilibrium) and the final time of the simulation.

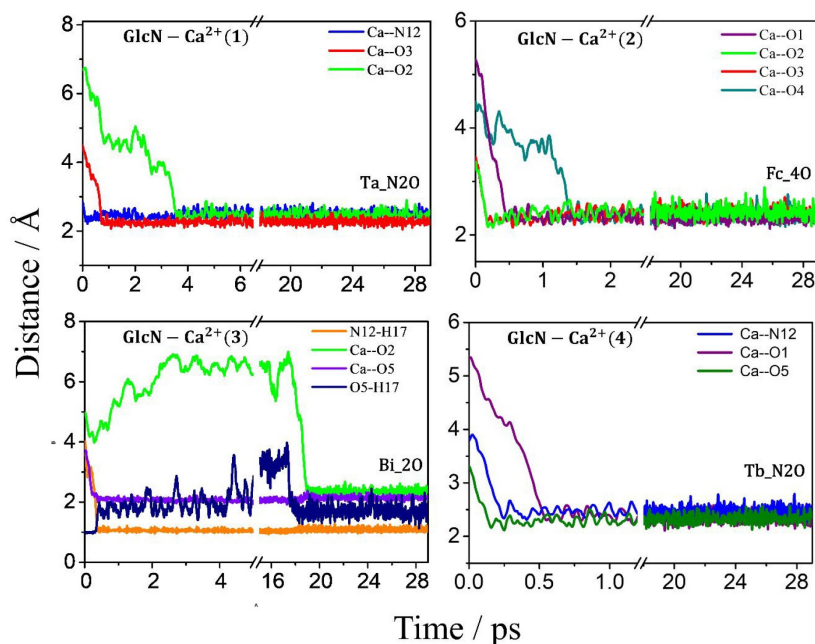


Figure 3. The bond lengths formed between the sites of glucosamine and Ca²⁺ and the broken bonds are reported as a function of time for the trajectories of the four different initial configurations GlcN-Ca²⁺ (1), GlcN-Ca²⁺ (2), GlcN-Ca²⁺ (3), and GlcN-Ca²⁺ (4) at 300 K.

Microsolvation

The two initial configurations that led to the most stable complexes in gas-phase simulations were selected (GlcN-Ca²⁺ (2) and GlcN-Ca²⁺ (3)) to study the role of water solvation in the interaction of the capture of a calcium ion by GlcN. In each one of the nanoreactors, 12 H₂O molecules were added. Figure 4 shows the structures obtained by microsolvation simulations. The complex formed (Hp_{30_4W}) by the microsolvation started from GlcN-Ca²⁺ (2) presented four interactions with water molecules and three with hydroxyl groups of the GlcN, given a calcium coordination number of seven. The interactions of this complexation started when the calcium ion approached O2 and O3 almost simultaneously (0.01 ps); shortly after that, three water molecules approached about 0.145, 0.290, and 0.435 ps. Only after 4 ps that O1 of GlcN and the fourth water molecule bound with the calcium ion. In our previous study,⁵² in which we simulated the water solvation of GlcN molecule using *ab initio* molecular dynamics, the results showed that the water molecules formed interactions with different sites of GlcN. Here, we also found a similar behavior; for instance, the H21 and N12 atoms of GlcN interacted with the oxygen and hydrogen from a water molecule during the simulation.

It was observed in the second trajectory, from the GlcN-Ca²⁺ (3) initial configuration that the complex formation began at 0.17 ps when O5 and a water molecule approached the calcium ion, forming two interactions in the opposite direction. A tridentate complex was created by the

interaction of the second water molecule at about 0.21 ps. The third water was complexed at about 2.05 ps. It was only at about 5.04 ps that O4 and the fourth water molecule interacted with the calcium ion in opposite directions, forming a hexacoordinate complex (Hx_{20_4W}) that remained until the end simulation. It is worth mentioning that the intramolecular hydrogen transfer between the hydroxyl group and the amino group of GlcN was not observed in the microsolvation environment, as occurred in the gas-phase environment, since water molecules modified

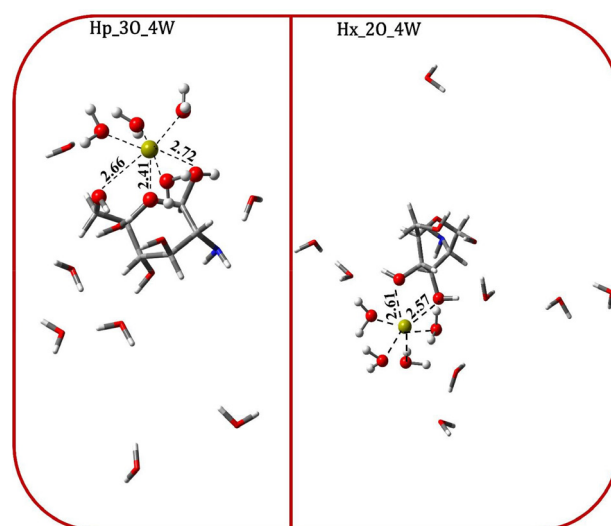


Figure 4. The geometrical parameters of the complexes formed between the calcium ion and glucosamine in a microsolvation environment by Car-Parrinello Molecular Dynamics. The coordination bond lengths correspond to the average distance / Å, of the interaction between the initial time of complex formation and the final time of the simulation.

the geometric parameters of GlcN, thus avoiding the approximation of hydroxyl hydrogen to the amino group.

The interaction energies of Hp_3O_4W and Hx_2O_4W were, respectively, -718.99 and -429.52 kJ mol $^{-1}$, suggesting that the microsolvation process promotes a decrease of 75.54 and 352.08 kJ mol $^{-1}$, respectively, in the interaction energies between the GlcN and the calcium ion.

Helmholtz free energy

The Helmholtz free energies were estimated using equation 4:

$$F = -K_B T \ln[P(\Delta r)] \quad (4)$$

where F and K_B stand for Helmholtz free energy and Boltzmann constant, respectively. T and $P(\Delta r)$ represent the system temperature and the hydrogen bond length distribution function, respectively.

Figure 5 shows Helmholtz's free energies (F) calculated

for the four trajectories between GlcN and Ca $^{2+}$ interactions. In the Ta_N2O, the interaction that showed the most stable Helmholtz's free energy was the Ca--O3, with an energy barrier estimated in $\Delta F = -16$ kJ mol $^{-1}$. The Ca--O2 and Ca--N12 interactions showed flat energy barriers, with values around -12 kJ mol $^{-1}$. In the Fc_4O complex, the energy of the four interactions were similar, with values of about -16 kJ mol $^{-1}$. In the Bi_2O complex, the Ca--O5 interaction was more stable than the Ca--O2 interaction, the energy barriers were estimated at -20 and -16 kJ mol $^{-1}$, respectively. The energy barriers for the Tb_N2O complex were estimated around -16 kJ mol $^{-1}$ for each interaction (see Figure 5).

Figure 6 shows Helmholtz's free energy of the interactions between GlcN and Ca $^{2+}$ for two complex structures formed in microsolvated environment. For the Hp_3O_4W complex, the interaction Ca--O1 showed to be the most stable with a free energy barrier around -16 kJ mol $^{-1}$. The interactions Ca--O2 and Ca--N12 showed flat energy barriers with values about -12 kJ mol $^{-1}$.

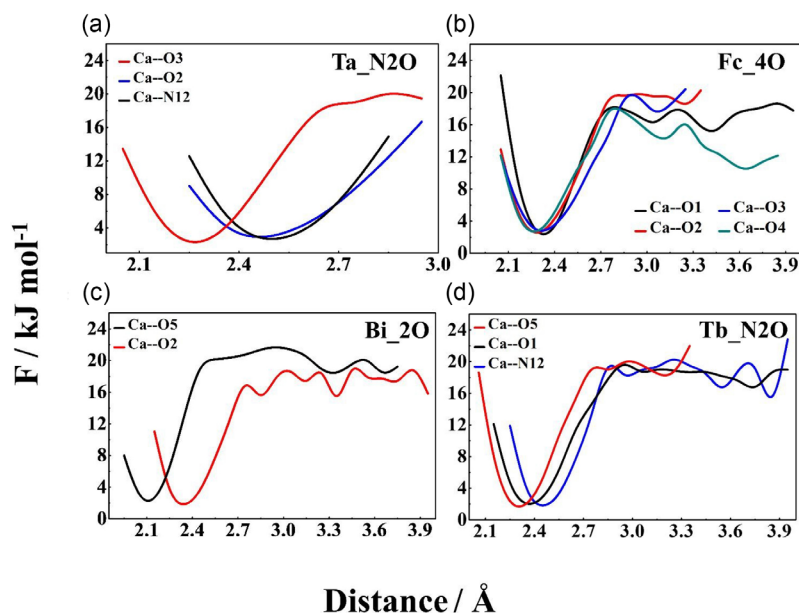


Figure 5. Helmholtz's free energies (F) for the interaction between GlcN and Ca $^{2+}$ for the complexes (a) Ta_N2O, (b) Fc_4O, (c) Bi_2O, and (d) Tb_N2O in gas-phase.

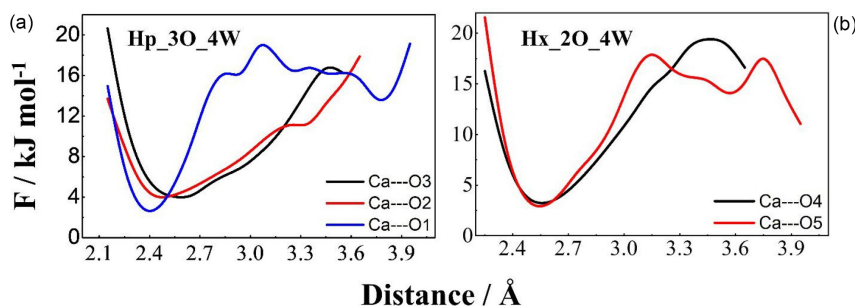


Figure 6. Helmholtz's free energy (F) for the interaction between GlcN and Ca $^{2+}$ for the complexes (a) Hp_3O_4W and (b) Hx_2O_4W.

In the Hx_2O_4W, the energies of the Ca---O4 and Ca---O5 interactions had similar values about -16 kJ mol^{-1} . Therefore, the formation of the two complexes is energetically favorable.

Quantum theory of atoms in molecules

The ability of Bader's Quantum theory of Atoms in Molecules (QTAIM)⁴⁹ to explore and characterize the nature of the atom-atom interactions in a molecular system in terms of properties of electronic density at bond critical points (BCP) is well documented.^{53,54} The signs and values of the Laplacian electron density, $\nabla^2\rho(\mathbf{r})$, and the electron density, $\rho(\mathbf{r})$, at the corresponding BCP are in accordance with the following conditions:⁴⁹ (i) $100 < 0.1$ and $\nabla^2\rho(\mathbf{r}) >$

0 as closed-shell interactions such as hydrogen bonds, van der Waals interactions, and ionic bonds;⁵⁵ (ii) $\rho(\mathbf{r}) > 0.2$ and $\nabla^2\rho(\mathbf{r}) < 0$ indicate predominantly covalent interactions. The magnitude of $\rho(\mathbf{r})$ reflects the "degree of covalency" present in each interaction, i.e., increases in values of $\rho(\mathbf{r})$ lead to a higher covalent character of the interaction.

For each of the complexes, two non-correlated snapshots of each interaction between GlcN and the calcium cation were selected to obtain the range in which the density and the Laplacian vary throughout the simulation time: one corresponding to the shortest distance bond and the other to the longest distance bond. Table 1 and Figure S1 (Supplementary Information section) show the topological properties of electronic density in the BCP of each interaction, distance bond,

Table 1. Distances simulation, time and topological parameters of the electron density, calculated at the M06-2X/6-31G** level of theory

Interaction	Simulation time / ps	Distance / Å	$\rho(\mathbf{r})$ / a.u.	$G(\mathbf{r})$ / a.u.	$V(\mathbf{r})$ / a.u.	$\nabla^2\rho(\mathbf{r})$ / a.u.	$ V(\mathbf{r}) /G(\mathbf{r})$ / a.u.
Fc_4O							
Ca ²⁺ ...O1	18.795	2.096	0.060	0.107	-0.099	0.459	0.928
	15.868	2.645	0.016	0.021	-0.017	0.098	0.808
Ca ²⁺ ...O2	9.818	2.149	0.050	0.088	-0.078	0.387	0.896
	6.727	2.756	0.011	0.014	-0.010	0.069	0.752
Ca ²⁺ ...O3	30.926	2.164	0.048	0.083	-0.074	0.369	0.892
	27.870	2.891	–	–	–	–	–
Ca ²⁺ ...O4	29.219	2.153	0.050	0.087	-0.078	0.383	0.898
	24.073	2.776	0.011	0.014	-0.010	0.069	0.757
Bi_2O							
Ca ²⁺ ...O2	22.97	2.125	0.062	0.089	-0.083	0.376	0.940
	29.96	2.687	0.017	0.017	-0.014	0.077	0.847
Ca ²⁺ ...O5	27.79	1.977	0.095	0.138	-0.143	0.527	1.043
	33.59	2.352	0.042	0.044	-0.042	0.186	0.955
Ta_N2O							
Ca ²⁺ ...O2	14.594	2.237	0.0471	0.062	-0.056	0.274	0.901
	27.463	2.895	0.0110	0.010	-0.008	0.045	0.829
Ca ²⁺ ...O3	18.152	2.014	0.0808	0.123	-0.122	0.498	0.988
	15.210	2.548	0.0233	0.024	-0.021	0.110	0.854
Ca ²⁺ ...N12	8.932	2.265	0.0544	0.062	-0.061	0.249	0.993
	17.126	2.859	0.0166	0.012	-0.011	0.053	0.914
Tb_N2O							
Ca ²⁺ ...O1	13.75	2.108	0.069	0.095	-0.092	0.389	0.974
	13.592	2.809	0.015	0.013	-0.012	0.056	0.908
Ca ²⁺ ...O5	6.305	2.086	0.057	0.073	-0.069	0.310	0.944
	15.341	2.635	0.020	0.019	-0.017	0.087	0.861
Ca ²⁺ ...N12	14.250	2.246	0.058	0.066	-0.066	0.260	1.007
	27.838	2.793	0.020	-0.014	-0.014	0.064	0.931

$\rho(\mathbf{r})$: electron density; $G(\mathbf{r})$: kinetic energy; $V(\mathbf{r})$: potential energy; $\nabla^2\rho(\mathbf{r})$: Laplacian; Fc_4O: complex with four coordination oxygen; Bi_2O: bidentate complex with two oxygen; Ta_N2O: first tridentate complex with one nitrogen and two oxygen; Tb_N2O: second tridentate complex one nitrogen and two oxygen.

and the time of the simulation in which the properties were investigated.

Except for the longest distance for the Ca--O3 interaction of the Fc_4O, in all other interactions of four complexes, the presence of BCP was seen. For the longest distances, the density found a range between 0.01 and 0.042 a.u. with positive Laplacians, and for the shortest distances, a range between 0.048 to 0.095 au was observed, also with positive Laplacians revealing a closed-shell character for all interactions observed in all four complexes.

The ionic character of the interactions was carried out by the ratio of the potential energy module and kinetic energy in critical point: $|V(\mathbf{r})|/G(\mathbf{r})$, e.g., if values of $|V(\mathbf{r})|/G(\mathbf{r}) < 1$ showed a predominant ionic nature; if $1 < |V(\mathbf{r})|/G(\mathbf{r}) < 2$, a partially covalent nature, and if $|V(\mathbf{r})|/G(\mathbf{r}) > 2$ a covalent

nature.^{49,56} The interactions showed values of $|V(\mathbf{r})|/G(\mathbf{r})$ in the range between 0.752 and 1.043, revealing an ionic nature. Only two interactions N12 in Tb_N2O and Ca--O5 in Bi_2O showed values $1 < |V(\mathbf{r})|/G(\mathbf{r}) < 2$, both in the shortest interaction distance; however, these values were very close to 1, which leads us to believe that they also have a predominantly ionic character.

Both complexes formed in the microsolvation environment indicated the presence of BCP, except for the longest distance of the Ca--O2 and Ca--O3 of the Hp_3O_4W complex and Ca--w1 and Ca--w3 of the Hx_O2_W4 complex. The range of the electronic density varying from 0.005 to 0.014 au with positive Laplacians, and for the shortest distances varying from 0.020 to 0.058 a.u. (see Table 2), also with positive Laplacians, revealing the closed-shell character for all interactions. The

Table 2. Distances simulation, time and topological parameters of the electron density calculated at the M06-2X/6-31G** level of theory

Interaction	Simulation time / ps	Distance / Å	$\rho(\mathbf{r})$ / a.u.	$G(\mathbf{r})$ / a.u.	$V(\mathbf{r})$ / a.u.	$\nabla^2\rho(\mathbf{r})$ / a.u.	$ V(\mathbf{r}) /G(\mathbf{r})$ / a.u.
Hp_3O_4W							
Ca ²⁺ ...O1	31.477	2.144	0.058	0.084	-0.078	0.359	0.929
	30.947	2.742	0.014	0.014	-0.012	0.067	0.857
Ca ²⁺ ...O2	17867	2.187	0.054	0.074	-0.068	0.323	0.919
	20.174	3.580	–	–	–	–	–
Ca ²⁺ ...O3	11.459	2.263	0.043	0.058	-0.051	0.257	0.879
	17.805	3.593	–	–	–	–	–
Ca ²⁺ ...Ow1	29.903	2.185	0.020	0.020	-0.017	0.095	0.850
	23.128	2.923	0.009	0.008	-0.007	0.041	0.875
Ca ²⁺ ...Ow2	21.843	2.127	0.022	0.024	-0.020	0.114	0.833
	29.651	2.915	0.011	0.009	-0.008	0.043	0.889
Ca ²⁺ ...Ow3	12.056	2.160	0.033	0.040	-0.034	0.184	0.850
	6.203	2.935	0.009	0.008	-0.007	0.040	0.875
Ca ²⁺ ...Ow4	21.375	2.168	0.054	0.078	-0.071	0.338	0.910
	11.455	3.171	0.005	0.005	-0.004	0.024	0.800
Hx_2O_4W							
Ca ²⁺ ...O4	19.476	2.296	0.043	0.053	-0.048	0.234	0.906
	25.989	3.035	0.009	0.007	-0.006	0.033	0.857
Ca ²⁺ ...O5	26.189	2.256	0.046	0.060	-0.054	0.263	0.900
	8.003	3.262	0.005	0.004	-0.003	0.021	0.750
Ca ²⁺ ...Ow1	24.431	2.244	0.045	0.060	-0.053	0.268	0.883
	28.329	3.057	–	–	–	–	–
Ca ²⁺ ...Ow2	9.537	2.275	0.045	0.056	-0.050	0.250	0.893
	5.871	2.992	0.030	0.005	0.004	0.001	0.800
Ca ²⁺ ...Ow3	29.052	2.262	0.044	0.057	-0.051	0.255	0.895
	21.816	3.192	–	–	–	–	–
Ca ²⁺ ...Ow4	10.606	2.274	0.044	0.056	-0.050	0.248	0.893
	18.236	3.157	0.006	0.005	-0.004	0.025	0.800

$\rho(\mathbf{r})$: electron density; $G(\mathbf{r})$: potential kinetic energy; $V(\mathbf{r})$: energy; $\nabla^2\rho(\mathbf{r})$: Laplacian; Hp_3O_4W: heptacoordinate complex, being 3 oxygen and 4 water molecules; Hp_2O_4W: hexacoordinate complex, being 2 oxygen and 4 water molecules.

ratio values $|V(\mathbf{r})|/G(\mathbf{r})$ are less than 1, showing the ionic nature of these interactions. Furthermore, it is noteworthy that due to lower electronic densities observed in these interactions, as compared with those in complexes formed in the gas-phase, it is estimated that the complexes with water molecules have a stronger ionic character.

Natural bond orbital analysis

To identify the most important orbitals involved in the ionic interactions of these complexes, the NBO analysis was carried out using the M06-2X/6-311++G(d,p) level of theory. The NBO analysis was performed by taking the snapshot that showed the lowest complexation energy during the simulations. The most important values of energy

Table 3. The most important second-order interaction energies, between the donor and acceptor NBOs for each complex between GlcN and calcium cation in gas-phase

Donor NBO (<i>i</i>)	Acceptor NBO (<i>j</i>)	$E^{(2)}$ / (kJ mol ⁻¹)
Fc_O4		
$n_2(O1)$	$n_1^*(Ca)$	41.88
$n_2(O2)$	$n_1^*(Ca)$	27.32
$n_2(O2)$	$n_3^*(Ca)$	22.93
$n_2(O3)$	$n_1^*(Ca)$	30.88
$n_2(O3)$	$n_2^*(Ca)$	27.70
$n_2(O4)$	$n_1^*(Ca)$	37.82
$n_2(O4)$	$n_2^*(Ca)$	28.45
Bi_O2		
$n_2(O2)$	$n_2^*(Ca)$	22.01
$n_1(O2)$	$n_2^*(Ca)$	17.91
$n_1(O5)$	$n_3^*(Ca)$	25.31
$n_2(O5)$	$n_2^*(Ca)$	15.34
Ta_NO2		
$n_1(N12)$	$n_1^*(Ca)$	64.06
$n_2(O2)$	$n_2^*(Ca)$	31.59
$n_2(O2)$	$n_3^*(Ca)$	24.60
$n_2(O3)$	$n_1^*(Ca)$	37.57
$n_2(O3)$	$n_2^*(Ca)$	32.13
$n_2(O3)$	$n_3^*(Ca)$	64.06
Tb_NO2		
$n_1(N12)$	$n_1^*(Ca)$	66.07
$n_2(O1)$	$n_2^*(Ca)$	35.10
$n_2(O1)$	$n_1^*(Ca)$	27.24
$n_2(O5)$	$n_3^*(Ca)$	40.58
$n_2(O5)$	$n_1^*(Ca)$	9.70

NBO: Natural Bond Orbital; *n*: lone pair of electrons; n^* : empty orbitals; $E^{(2)}$: second-order interaction energies; Fc_4O: complex with four coordination oxygen; Bi_2O: bidentate complex with two oxygen; Ta_N2O: first tridentate complex with one nitrogen and two oxygen; Tb_N2O: second tridentate complex one nitrogen and two oxygen.

are given in Table 3 for complexes in the gas phase and Table 4 for complexes in the microsolvation environment. The NBO analyses (Table 3) showed that interactions of GlcN with the calcium cation result mainly from charge transfer from *n* lone pairs of the orbital of oxygen and nitrogen atoms from GlcN into the n^* empty orbitals of the calcium cation. For instance, the higher hyperconjugation energies for Fc_4O were $n_2(O1) \rightarrow n_1^*(Ca)$, $n_2(O2) \rightarrow n_1^*(Ca)$, $n_2(O3) \rightarrow n_1^*(Ca)$ and $n_2(O4) \rightarrow n_1^*(Ca)$, with stabilization energies of 41.88, 22.93, 30.88, and 37.82 kJ mol⁻¹, respectively. The highest donations of electron densities were observed from lone pairs of the nitrogen atom on the Ta_N2O and Tb_N2O complexes, with stabilization energies of 64.06 and 66.07 kJ mol⁻¹, respectively.

The formation of complexes in the water environment are governed by interactions of lone pairs of the orbital of oxygen and nitrogen atoms from GlcN and the lone pair

Table 4. The most important second-order interaction energies, $E^{(2)}$ between the donor and acceptor NBOs for each complex between GlcN and calcium cation in microsolvation environment

Donor NBO (<i>i</i>)	Acceptor NBO (<i>j</i>)	$E^{(2)}$ / (kJ mol ⁻¹)
Hp_3O_4W		
$n_2O(2)$	n_1^*Ca	63.51
$n_2O(2)$	n_1^*Ca	37.14
$n_2O(2)$	n_2^*Ca	34.29
$n_2O(3)$	n_1^*Ca	51.54
$n_2O(3)$	n_3^*Ca	42.83
$n_2O(w1)$	n_1^*Ca	60.83
$n_2O(w1)$	n_2^*Ca	46.60
$n_2O(w2)$	n_2^*Ca	46.85
$n_2O(w2)$	n_1^*Ca	68.79
$n_2O(w3)$	n_3^*Ca	71.26
$n_2O(w3)$	n_3^*Ca	30.06
$n_2O(w4)$	n_4^*Ca	48.23
$n_2O(w4)$	n_4^*Ca	53.51
Hx_2O_4W		
$n_2O(4)$	n_1^*Ca	32.32
$n_2O(4)$	n_2^*Ca	34.21
$n_2O(4)$	n_4^*Ca	29.81
$n_2O(5)$	n_2^*Ca	43.33
$n_2O(w1)$	n_1^*Ca	57.57
$n_2O(w1)$	n_4^*Ca	33.12
$n_2O(w2)$	n_2^*Ca	48.90
$n_2O(w3)$	n_1^*Ca	48.32
$n_2O(w3)$	n_3^*Ca	44.63
$n_2O(w4)$	n_3^*Ca	67.74

NBO: Natural Bond Orbital; *n*: lone pair of electrons; n^* : empty orbitals; $E^{(2)}$: second-order interaction energies; Hp_3O_4W: heptacoordinate complex, being 3 oxygen and 4 water molecules. Hp_2O_4W: hexacoordinate complex, being 2 oxygen and 4 water molecules.

orbital of an oxygen atom from water molecules into the n^* empty orbitals of the calcium cation, i.e., the highest hyperconjugation energy was $n_2\text{O}(w3) \rightarrow n_3^*(\text{Ca})$ with stabilization energy of $71.26 \text{ kJ mol}^{-1}$. The heptadentate complex shows higher hyperconjugation energy, which explains its higher energy of complexation and stability, leading us to believe this would be the most favorable structure in a reaction environment.

The NBO-derived charge of the calcium ion was estimated in both the gas phase and microsolvation environment. The average charge values of the calcium ion, for the frames with the shortest distances between interactions (Ca_O1, Ca_O2, and Ca_O3) in Fc_O4 and Hp_3O_4W, were 1.797 (Ca1.797+) in Fc_O4 and 1.619 (Ca1.619+) in Hp_3O_4W. Consequently, it can be concluded that water molecules transfer charges to the calcium ion.

Molecular orbital analysis

Figure 7 illustrates the frontier molecular orbitals, HOMO (highest occupied molecular orbital) and LUMO (lowest unoccupied molecular orbital). The energies of these orbitals and the difference between them ($\text{Gap} = E_{\text{LUMO}} - E_{\text{HOMO}}$) are crucial parameters for determining electronic properties and reactivity of molecules, including chemical potential and chemical

hardness. The ionization potential, $I \approx -E_{\text{HOMO}}$, and electron affinity, $A \approx -E_{\text{LUMO}}$, are related to the energy difference between the HOMO and LUMO orbitals. Molecules with larger gap values are typically hard and stable, whereas those with smaller gap values are often soft and reactive.⁵⁷ The energy gaps for the frame with the smallest distance of interaction between the Ca and O1 atoms in Fc_4O (Figure 7a) and Hp_3O_4W (Figure 7b) were 282.410 and $150.985 \text{ kcal mol}^{-1}$, respectively. Therefore, compared to GlcN complex in the gas-phase and microsolvation environments, GlcN complex in the gas-phase environment is more stable. It is interesting to note that the LUMO orbital energy is significantly negative for both complexes. This occurs because our analysis does not consider the presence of counter ions, as our primary focus is to investigate the interaction between the calcium ion and GlcN.

Conclusions

The Car-Parrinello molecular dynamics and density functional theory were employed to investigate the interactions between GlcN and calcium ions in gas-phase and aqueous microsolvation environments. The simulations demonstrated that stable $\text{GlcN} \cdots \text{Ca}^{2+}$ complexes can form at various sites on GlcN, mainly with hydroxyl and amino groups. The complexation energy in the gas-phase ranges from -680.50 to $-794.53 \text{ kJ mol}^{-1}$. QTAIM analyses

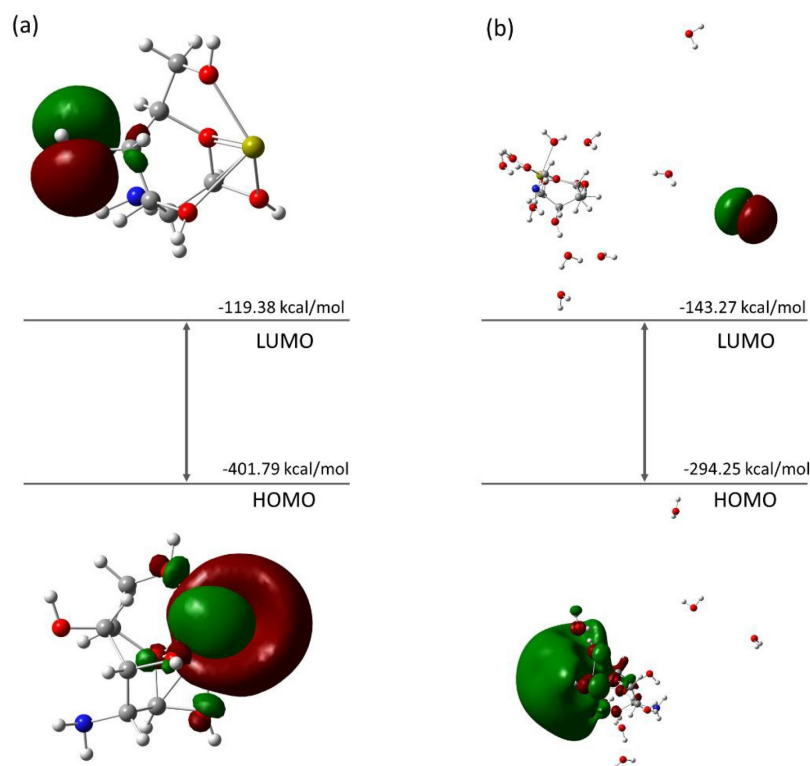


Figure 7. The HOMO and LUMO plot for (a) Fc_4O (b) Hp_3O_4W, calculated at M06-2X/6-311++G(d,p) level of theory.

revealed a closed-shell character for all interactions, while NBO analyses indicated that they mainly arise from charge transfer between the n lone pairs of the oxygen and nitrogen atoms from GlcN to the empty n orbitals of the calcium cation.

The microsolvation simulations showed that the presence of water molecules does not inhibit GlcN's interaction with the calcium ion, but rather decreases the complexation energies, especially for the Hx_2O_4W complex. QTAIM analyses demonstrated that all interactions remain ionic, as observed in the gas-phase environment. NBO analyses revealed that all interactions are governed by interactions of lone pairs from oxygen and nitrogen atoms of GlcN and lone pairs from oxygen atoms of water molecules with the empty n orbitals of the calcium ion. The Helmholtz's free energies indicated that GlcN–Ca²⁺ interactions are energetically favorable in both gas-phase and microsolvation environments. Given GlcN's extensive biological activities, a microscopic understanding of GlcN–Ca²⁺ complexation can guide new investigations and applications of GlcN in developing novel therapeutic applications.

Supplementary Information

Supplementary information is available free of charge at <http://jbcs.s bq.org.br> as PDF file.

Acknowledgments

The authors gratefully acknowledge financial support from FAPEG (Fundação de Ampara à Pesquisa do Estado de Goiás). We also thank the High-Performance Computing Center of the State University of Goiás for extensive computer support.

References

- Monteith, G. R.; McAndrew, D.; Faddy, H. M.; Roberts-Thomson, S. J.; *Nat. Rev. Cancer* **2007**, *7*, 519. [Crossref]
- Azimi, I.; Roberts-Thomson, S. J.; Monteith, G. R.; *Br. J. Pharmacol.* **2014**, *171*, 945. [Crossref]
- Nguyen, R. L.; Medvedeva, Y. V.; Ayyagari, T. E.; Schmunk, G.; Gargus, J. J.; *Biochim. Biophys. Acta, Mol. Cell Res.* **2018**, *1865*, 1718. [Crossref]
- Shanahan, C. M.; Crouthamel, M. H.; Kapustin, A.; Giachelli, C. M.; *Circ. Res.* **2011**, *109*, 697. [Crossref]
- Aune, D.; Navarro Rosenblatt, D. A.; Chan, D. S. M.; Vieira, A. R.; Vieira, R.; Greenwood, D. C.; Vatten, L. J.; Norat, T.; *Am. J. Clin. Nutr.* **2015**, *101*, 87. [Crossref]
- Park, J. H.; Kim, J. N.; Jang, B. C.; Im, S. S.; Song, D. K.; Bae, J. H.; *Environ. Toxicol. Pharmacol.* **2016**, *42*, 1. [Crossref]
- Liu, J.; Pang, Y.; Chang, T.; Bounelis, P.; Chatham, J. C.; Marchase, R. B.; *J. Mol. Cell. Cardiol.* **2006**, *40*, 303. [Crossref]
- Yampolsky, P.; Koenen, M.; Mosqueira, M.; Geschwill, P.; Nauck, S.; Witzemberger, M.; Seyler, C.; Fink, T.; Kruska, M.; Bruehl, C.; Schwoerer, A. P.; Ehmke, H.; Fink, R. H. A.; Draguhn, A.; Thomas, D.; Katus, H. A.; Schweizer, P. A.; *Nat. Commun.* **2019**, *10*, 3295. [Crossref]
- Chiandotti, R. S.; Rodrigues, P. C.; Akcelrud, L.; *J. Braz. Chem. Soc.* **2010**, *21*, 1910. [Crossref]
- Kaur, S.; Dhillon, G. S.; *Crit. Rev. Microbiol.* **2014**, *40*, 155. [Crossref]
- Younes, I.; Rinaudo, M.; *Mar. Drugs* **2015**, *13*, 1133. [Crossref]
- Ali, A.; Ahmed, S.; *Int. J. Biol. Macromol.* **2018**, *109*, 273. [Crossref]
- Ahsan, S. M.; Thomas, M.; Reddy, K. K.; Sooraparaju, S. G.; Asthana, A.; Bhatnagar, I.; *Int. J. Biol. Macromol.* **2018**, *110*, 97. [Crossref]
- Chen, M.-X.; Li, B.-K.; Yin, D.-K.; Liang, J.; Li, S.-S.; Peng, D.-Y.; *Carbohydr. Polym.* **2014**, *111*, 298. [Crossref]
- Hernández, R. B.; Yola, O. R.; Mercê, A. L. R.; *J. Braz. Chem. Soc.* **2007**, *18*, 1388. [Crossref]
- Zhu, B.; He, H.; Guo, D.; Zhao, M.; Hou, T.; *Food Hydrocoll.* **2020**, *102*, 105567. [Crossref]
- Gonzag, M. L. C.; Campelo, M. S.; Saraiva, K. B.; Santos, A. Q. S.; Leal, L. K. A. M.; Ricardo, N. M. P. S.; Soares, S. A.; Ribeiro, M. E. N. P.; *J. Braz. Chem. Soc.* **2020**, *31*, 990. [Crossref]
- Huang, B.; Liu, M.; Zhou, C.; *Carbohydr. Polym.* **2017**, *175*, 689. [Crossref]
- Escárcega-Galaz, A. A.; Sánchez-Machado, D. I.; López-Cervantes, J.; Sanches-Silva, A.; Madera-Santana, T. J.; Paseiro-Losada, P.; *Int. J. Biol. Macromol.* **2018**, *116*, 472. [Crossref]
- Liverani, L.; Lacina, J.; Roether, J. A.; Boccardi, E.; Killian, M. S.; Schmuki, P.; Schubert, D. W.; Boccaccini, A. R.; *Bioact. Mater.* **2018**, *3*, 55. [Crossref]
- Zhang, L.; Zeng, Y.; Cheng, Z.; *J. Mol. Liq.* **2016**, *214*, 175. [Crossref]
- Burakov, A. E.; Galunin, E. V.; Burakova, I. V.; Kucherova, A. E.; Agarwal, S.; Tkachev, A. G.; Gupta, V. K.; *Ecotoxicol. Environ. Saf.* **2018**, *148*, 702. [Crossref]
- Vieira, C. L.; Sanches Neto, F. O.; Carvalho-Silva, V. H.; Signini, R.; *J. Environ. Chem. Eng.* **2019**, *7*, 103070. [Crossref]
- Zahedipour, F.; Dalirfardouei, R.; Karimi, G.; Jamialahmadi, K.; *Biomed. Pharmacother.* **2017**, *95*, 1051. [Crossref]
- Dalirfardouei, R.; Karimi, G.; Jamialahmadi, K.; *Life Sci.* **2016**, *152*, 21. [Crossref]
- Towheed, T.; Maxwell, L.; Tp, A.; Shea, B.; Jb, H.; Welch, V.; Mc, H.; Ga, W.; *Cochrane Database Syst. Rev. Glucosamine* **2009**, *1*. [Crossref]
- Wu, S.; Dai, X.; Shilong, F.; Zhu, M.; Shen, X.; Zhang, K.; Li, S.; *Food Sci. Biotechnol.* **2018**, *27*, 1. [Crossref]

28. Terreux, R.; Domard, M.; Viton, C.; Domard, A.; *Biomacromolecules* **2006**, *7*, 31. [Crossref]
29. Fattahi, A.; Ghorat, M.; Pourjavadi, A.; Kurdtabar, M.; Torabi, A. A.; *Sci. Iran.* **2008**, *15*, 422. [Crossref]
30. Gomes, J. R. B.; Jorge, M.; Gomes, P.; *J. Chem. Thermodyn.* **2014**, *73*, 121. [Crossref]
31. Hassan, B.; Muraleedharan, K.; Abdul Mujeeb, V. M.; *Int. J. Biol. Macromol.* **2015**, *74*, 483. [Crossref]
32. Hassan, B.; Rajan, V. K.; Mujeeb, V. M. A.; Muraleedharan, K.; *Int. J. Biol. Macromol.* **2017**, *99*, 549. [Crossref]
33. Jeremić, S.; Tran, T. H.; Marković, Z.; Ngo, T. C.; Dao, D. Q.; *Comput. Theor. Chem.* **2018**, *1138*, 99. [Crossref]
34. Kotena, Z. M.; Fattahi, A.; *J. Mol. Graphics Modell.* **2020**, *98*, 107612. [Crossref]
35. Virués, C.; Hernández, J.; Higuera-Ciapara, I.; Martínez-Benavidez, E.; Olivares-Romero, J. L.; Navarro, R. E.; Inoue, M.; *Carbohydr. Res.* **2020**, *490*, 107952. [Crossref]
36. CPMD, IBM Corp, 1990-2015, MPI Fur Festkörperforschung Stuttgart, 1997-2001. [Link] accessed in January 2024
37. Kohn, W.; Sham, L. J.; *Phys. Rev.* **1965**, *140*, A1133. [Crossref]
38. Perdew, J. P.; Burke, K.; Ernzerhof, M.; *Phys. Rev. Lett.* **1996**, *77*, 3865. [Crossref]
39. Troullier, N.; Martins, J. L.; *Phys. Rev. B* **1991**, *43*, 1993. [Crossref]
40. Hutter, J.; Lüthi, H. P.; Parrinello, M.; *Comput. Mater. Sci.* **1994**, *2*, 244. [Crossref]
41. Nosé, S.; *Mol. Phys.* **1984**, *52*, 255. [Crossref]
42. Hoover, W. G.; *Phys. Rev. A* **1985**, *31*, 1695. [Crossref]
43. Machado, H. G.; Sanches-Neto, F. O.; Coutinho, N. D.; Mundim, K. C.; Palazzetti, F.; Carvalho-Silva, V. H.; *Molecules* **2019**, *24*, 3478. [Crossref]
44. *Mphyschem*, <http://www.mphyschem.com/transitivity>, accessed in January 2024.
45. Frisch, M. J.; Trucks, G. W.; Schlegel, H. B.; Scuseria, G. E.; Robb, M. A.; Cheeseman, J. R.; Scalmani, G.; Barone, V.; Mennucci, B.; Petersson, G. A.; Nakatsuji, H.; Caricato, M.; Li, X.; Hratchian, H. P.; Izmaylov, A. F.; Bloino, J.; Zheng, G.; Sonnenberg, J. L.; Hada, M.; Ehara, M.; Toyota, K.; Fukuda, R.; Hasegawa, J.; Ishida, M.; Nakajima, T.; Honda, Y.; Kitao, O.; Nakai, H.; Vreven, T.; Montgomery Jr., J. A.; Peralta, J. E.; Ogliaro, F.; Bearpark, M.; Heyd, J. J.; Brothers, E.; Kudin, K. N.; Staroverov, V. N.; Kobayashi, R.; Normand, J.; Raghavachari, K.; Rendell, A.; Burant, J. C.; Iyengar, S. S.; Tomasi, J.; Cossi, M.; Rega, N.; Millam, J. M.; Klene, M.; Knox, J. E.; Cross, J. B.; Bakken, V.; Adamo, C.; Jaramillo, J.; Gomperts, R.; Stratmann, R. E.; Yazyev, O.; Austin, A. J.; Cammi, R.; Pomelli, C.; Ochterski, J. W.; Martin, R. L.; Morokuma, K.; Zakrzewski, V. G.; Voth, G. A.; Salvador, P.; Dannenberg, J. J.; Dapprich, S.; Daniels, A. D.; Farkas, O.; Foresman, J. B.; Ortiz, J. V.; Cioslowski, J.; Fox, D. J.; *Gaussian 09*, Revision E.01; Gaussian, Inc., Wallingford CT, USA, 2009.
46. Zhao, Y.; Truhlar, D. G.; *Theor. Chem. Acc.* **2008**, *120*, 215. [Crossref]
47. Boys, S. F. F.; Bernardi, F.; *Mol. Phys.* **1970**, *19*, 553. [Crossref]
48. Faver, J. C.; Zheng, Z.; Merz, K. M.; *J. Chem. Phys.* **2011**, *135*, 144110. [Crossref]
49. Bader, R. F. W.; *Acc. Chem. Res.* **1985**, *18*, 9. [Crossref]
50. Reed, A. E.; Curtiss, L. A.; Weinhold, F.; *Chem. Rev.* **1988**, *88*, 899. [Crossref]
51. Lu, T.; Chen, F.; *J. Comput. Chem.* **2012**, *33*, 580. [Crossref]
52. Camargo, L. T. M.; Signini, R.; Catharina, A.; Rodrigues, C.; Lopes, Y. F.; Camargo, A. J.; **2020**, *124*, 6986. [Crossref]
53. Kumar, P. S. V.; Raghavendra, V.; Subramanian, V.; *J. Chem. Sci.* **2016**, *128*, 1527. [Crossref]
54. Lepetit, C.; Fau, P.; Fajerweg, K.; Kahn, M. L.; Silvi, B.; *Coord. Chem. Rev.* **2017**, *345*, 150. [Crossref]
55. Boyd, R. J.; Matta, F.; Boyd, R. J.; Matta, C. F.; Boyd, R. J.; *The Quantum Theory of Atoms in Molecules*; Wiley-VCH Verlag GmbH & Co. KGaA: Weinheim, Germany, 2007.
56. Astani, E. K.; Chen, N. C.; Huang, Y. C.; Bahrami, A.; Chen, L. Y.; Lin, P. R.; Guan, H. H.; Lin, C. C.; Chuankhayan, P.; Hadipour, N. L.; Chen, C. J.; *J. Mol. Graphics Modell.* **2017**, *78*, 61. [Crossref]
57. Parr, R. G.; Pearson, R. G.; *J. Am. Chem. Soc.* **1983**, *105*, 7512. [Crossref]

Submitted: November 23, 2022

Published online: February 27, 2024